Hindawi
International Journal of Electrochemistry
Volume 2019, Article ID 5392452, 11 pages
https://doi.org/10.1155/2019/5392452

Research Article

Straight-Parallel Electrodes and Variable Gap for Hydrogen and Oxygen Evolution Reactions

María J. Lavorante,[1] **Carla Y. Reynoso**,[2] **and Juan I. Franco**[1]

[1]*Departamento de Investigación y Desarrollo en Energías Renovables (DIDER), Instituto de Investigaciones Científicas y Técnicas para la Defensa (CITEDEF) San Juan Bautista de La Salle 4397 (B1603ALO), Villa Martelli, Buenos Aires Province, Argentina*
[2]*Escuela Superior Tecnica Grl. Div. Manuel N. Savio, Facultad de Ingenieria del Ejercito, Universidad de la Defensa. Av. Cabildo 15 (C1426AAA), Ciudad Autonoma de Buenos Aires, Argentina*

Correspondence should be addressed to María J. Lavorante; mjlavorante@gmail.com

Received 30 November 2018; Revised 8 May 2019; Accepted 13 June 2019; Published 1 August 2019

Academic Editor: Gerd-Uwe Flechsig

The challenges to be overtaken with alkaline water electrolysis are the reduction of energy consumption, the maintenance, and the cost as well as the increase of durability, reliability, and safety. Having these challenges in mind, this work focused on the reduction of the electrical resistance of the electrolyte which directly affects energy consumption. According to the definition of electrical resistance of an object, the reduction of the space between electrodes could lower the electrical resistance but, in this process, the formation of bubbles could modify this affirmation. In this work, the performance analyses of nine different spaces between stainless steel 316L electrodes were carried out, although the spaces proposed are not the same as those from the positive electrode (anode) to the separator and from the separator to the negative electrode (cathode). The reason why this is studied is that stoichiometry of the reaction states that two moles of hydrogen and one mole of oxygen can be obtained per every two moles of water. The proposed spaces were 10.65, 9.20, 8.25, 7.25, 6.30, 6.05, 4.35, 4.15, and 3.40 millimetres. From the nine different analysed distances between electrodes, it can be said that the best performance was reached by one of the smallest distances proposed, 4.15 mm. When the same distance between electrodes was compared (the same and different distance between electrodes and separator), the one that had almost twice the distance (negative compartment) presented an increase in current density of approximately 33% with respect to that where both distances (from electrodes to separator) are the same. That indicates that the stichometry of the electrolysis reaction influenced the performance.

1. Introduction

Hydrogen has long been considered as a clean energy vector because it can be used in fuel cells to produce electricity, water, and heat [1–4]. This vector can be produced by more than 90 different methods, where water electrolysis is one of the most promissory ones, mainly because its use at industrial, commercial, and military levels dates back to the 19th century, without neglecting its simplicity [5, 6]. This method offers numerous advantages as it does not generate polluting emissions for the environment; the gaseous products which are obtained, hydrogen and oxygen, have a high degree of purity, which makes them attractive for their use in fuel cells. The operation and shelf life of these batteries can be very strongly affected by impurities which the fuel and the oxidiser may contain when using other methods of production, thus needing different and expensive purification steps. Electrolysis is an electrochemical method that can be applied at different scales depending on the need or requirements of fuel, hydrogen.

The cost of this mechanism basically depends on the price of energy necessary to carry out the electrolysis and to maintain the electrolytic cell at working temperature. Energy constitutes the major share in the cost of this type of method. The production cost of hydrogen and oxygen using electrolysers depend on the cost of electrical energy. Electricity is known to be the most expensive form of energy. Its production has an average efficiency of around

30-40% with respect to the primary energy sources so, for the electrolyser, it is generally below 40% [7]. In most industrial electrolysers, the energy consumption is 4.5-5 kWh/Nm^3 n H_2 [7, 8].

This is the reason why the use of this type of technology could be more attractive when the source of energy is totally renewable. The type of energy sources will depend on the availability of the energy matrix where this technology is implemented.

The current research trends on alkaline water electrolysis include several aspects as electrodes, electrolytes, ionic transport, bubble formation, and departure. The challenges to be overtaken with this technology are twofold. One is the reduction of energy consumption, the maintenance, and the cost and, on the other hand, the increase of durability, reliability, and safety [9–11]. Another aspect to consider, although rarely taken into account, is making use of the cheapest possible electricity, while research improves the process. An example could be the excess of electrical energy during night or wind power.

With the objective to reduce the cost of the components of the electrolysers, a considerable number of researchers are focused on studying low cost materials or modifying those already existing to make this technology more affordable and trying to solve this pressing issue for industry.

In that direction P. Lettenmeier et al. worked in the development of a coated stainless steel bipolar plate for proton exchange membrane (PEM) electrolysers. The coating was made with titanium (Ti) using vacuum plasma spraying and then, with platinum (Pt) by magnetron sputtering physical vapor deposition. These bipolar plates were evaluated during 1000 hours in a commercial PEM electrolyser. Results suggest that on the cathode side, it is not necessary to coat the stainless steel with Ti because stainless steel 316L is more resistant to hydrogen embrittlement. In none of the bipolar plates studied was corrosion observed after 1000 hours. The highest performance was achieved when these two coatings were used for the bipolar plates. As a decrease in the performance of the electrolyser or some kind of degradation/corrosion in the substrate could not be observed, it was possible to say that stainless steel 316L can be used as base material for the manufacture of bipolar plates [12].

The work by M. Schalenbach et al., a simple physical model, which consists of analytical equations, is used to describe voltage-current characteristics, heat balance, hydrogen and oxygen crossover, and cell efficiency of acidic and alkaline water electrolysers. The model was parameterised with electrolyser cells which were designed and built as those that presented the best performance in literature [13, 14]. In relation to the voltage-current characteristic, a higher cell resistance of the alkaline water electrolyser was found. This is attributed to the use of a thicker separator and microporous electrodes in comparison with the acidic ones. The conductivities of both kinds of electrolysers are equal. This means that they have almost the same ohmic drops at the same distance between electrodes. Kinetics overvoltage was found to be 30% smaller for the acidic water electrolyser. Hydrogen diffusivity is 38-fold lower in the alkaline separator than in the Nafion® membrane. This analysis shows that the alkaline water electrolyser with nickel-based catalysts (Zirfon® filled with 30 wt% potassium hydroxide (KOH) solution) but using thinner separators than usual is expected to be more efficient than acidic with iridium (Ir) and platinum-based catalysts and Nafion® as a polymer electrolyte membrane [15].

In the research work by Kraglund et al., a ternary poly(2-2′-(m-phenylene)-5,5-bibenzimidazole (m-PBI) was prepared and systematically characterised, with respect to stability and performance. It was used as electrolyte in a zero-gap alkaline water electrolyser under the influence of different KOH concentration (from 5 to 30 wt %). After its synthesis the m-PBI membrane was tested in a laboratory cell consisting of flow field plates with a linear pattern, nickel (Ni) foam electrodes and poly(tetra-fluoroethylene) (PTFE) gasket and compared with Zirfon® diaphragm. When a concentration of 20-25 wt % aqueous KOH is analysed the best results are obtained. With 5, 15, and 30 wt % the operation of the electrolyser is stable but its subsequent analysis evidenced oxidative degradation of m-PBI in 15 and 30 wt % KOH [16].

Delvaux et al. studied morphologically controlled nickel thin film electrodes. Those nickel-aluminium alloy films, of different compositions, were obtained by magnetron cosputtering from nickel (Ni) and aluminium (Al) cathodes with a thickness of about 50 nm. Time and deposition power were modified in order to obtain different initial aluminium/nickel atomic ratios of 0; 0.2; 0.4 and 0.7. The aluminium was selectively leached in an ultrapure stagnant 30 wt % KOH solution at room temperature to produce the de-alloyed nickel electrodes. The results were used to provide a systematic understanding of the factors that improve bubble detachment from the electrode surfaces. The electrochemical measurements were made in a 25 mL PTFE cell in a flow through configuration with a 1.0 mol/L KOH solution as electrolyte. After the leaching step, little aluminium was leaked out and there was no change at the intermetallic phases, but the electrochemical performance in relation of the oxygen evolution reaction potential improved from the dealloyed nickel electrodes over the pure nickel one. The reason for those results was justified by the higher surface roughness measured of the de-alloyed electrodes that allow a better bubble detachment from their surface. This last affirmation was confirmed by cyclic voltammetry where forced convection had a higher influence in the potential for pure nickel than in de-alloyed electrodes [17].

In the research work presented by Lu et al., a new anode was developed and characterised for oxygen evolution reaction. The electrode consists of a hierarchically structured three-dimensional amorphous mesoporous nickel-iron composite nanosheet prepared by electrodeposition onto nickel foam substrates. The nickel-iron (NiFe) catalyst is uniformly deposited onto the macroscopic 3D skeleton of nickel foam, which proves to be a high catalyst loading and has large quantities of active sites. The NiFe deposits of rippled nanosheet structure are interconnected to form mesoporous nanostructure with 50 nm as the pore size. These amorphous nanosheets are highly transparent, which is indicative of their ultrathin condition. The composite obtained is $Ni_3Fe(OH)_9$ with an oxidation state for nickel Ni^{2+} and for iron Fe^{3+}. The

electrode presents high catalytic activity from the composite and the synergistic effect between nickel and iron. It has excellent mass transport properties, conductivity, and mechanical robustness. During electrolysis gas bubbles dissipate rapidly into the solution and its accumulation is not observed over the electrode surface. The deposit structure was well-preserved, which implies the nonrelease or dissolution of the catalyst from the substrate. This means that these electrodes are a promising alternative to the costly IrO_2 and RuO_2 oxygen evolution reaction catalysts and, to the nickel, cobalt-base composite, which usually require much higher overpotentials [18].

Trinke et al. focused their work on an important issue for PEM and alkaline water electrolysers: the hydrogen and oxygen crossover. The permeation of hydrogen into the anodic half-cell is of special relevance because an explosive gas mixture can be formed; but there are two further negative side effects of gas crossover: reduction of Faraday efficiency and degradation. In order to obtain comparable data, the experiments of both technologies were carried out with state-of-the-art separating unit materials: Nafion® 117 for PEM and Zirfon® for alkaline at a working temperature of 60°C. The crossover routes can be divided into diffusive and convective mass transfer mechanisms. With respect to diffusion, the products pass through the membrane or separator to get into the opposite half-cell compartment. Convection could be divided into further mechanisms such as differential pressure, electroosmotic drag, electrolyte mixing, and supersaturation [19].

In the differential pressure, the presence of total pressure gradients allows the transport of dissolved species and electrolyte across the separating unit. At the electroosmotic drag, the solvent can drag ions and dissolve gas across the separating unit due to the electric field. In PEM electrolysis, dissolved oxygen could be dragged with protons into the cathodic compartment or reduce hydrogen permeation. In alkaline electrolysis, hydroxide ions are responsible for the charge transport so, as they are transported from the cathodic to the anodic compartment, this may enhance hydrogen and reduce oxygen crossover. Before gas bubble grows, the gases are produced in dissolved form. Therefore, the electrolyte becomes supersaturated, that is to say, a higher concentration of dissolved hydrogen within the electrode boundary or catalyst layer. So, there are two competing mechanisms for the dissolved hydrogen mass transfer: transported to the electrolytic bulk in dissolved form or to the gas liquid interface of gas bubbles present in the electrode boundary layer. The results obtained in hydrogen as impurity of the anodic compartment show that, at higher current densities, a decrease of the hydrogen contamination is justified by a rising oxygen evolution rate that dilutes the permeating hydrogen and reduces its fraction. If the operating pressure is increased, the same happens with the content of hydrogen but, for PEM, it is much higher than in alkaline electrolysis. This affirmation changes if there is a mixing of anodic and cathodic electrolyte cycles. The rise of pressures, as the amount of dissolved gas within the electrolyte increases, decreases gas bubble diameter and complicates an adequate gas separation. So, the recirculation rate should be kept as low as possible but high enough to maintain the temperature increase and avoid a rise of the electrode bubble coverage. When hydrogen crossover was determined through Nafion® 117 membrane and Zirfon® separator as a function of current density, hydrogen crossover increased with rising of current density as well as the system pressure. In the case of PEM electrolysis, the linear dependency of hydrogen crossover on the current density is explained by mass transport resistances within cathode catalyst layer that cause an increasing supersaturation of dissolved hydrogen as the current density increases. In alkaline electrolysis hydrogen crossover initially increases with the current density until a plateau is reached. Rising system pressures seem to shift the formation of the plateau towards higher current densities. This effect was justified by hydrogen mass transfer coefficient from liquid electrolyte into gas phase at higher current densities. The works presented by Vogt [20], Chin Kwie Joe [21], and St-Pierre [22] with their respected coworkers showed that the gas evolution efficiency, at low current densities, had a strong rise, until a linear dependency was observed. When the current density is very small the total amount of products formed leaves the electrodes in a dissolved form. With the rising of current density, the concentration of dissolved hydrogen becomes high enough to activate nucleation sites, which allows the gas bubbles evolution at the electrodes. As the pressure increases, the gas evolution efficiency is displaced to higher current densities justifying the formation of the plateau.

So, comparing the two technologies diffusive crossover, it is more than one order of magnitude higher in PEM that in alkaline electrolysis, which is the main cause of the low solubility of hydrogen in concentrated potassium hydroxide.

As regards crossover breakdown for PEM electrolysis a small proportion of the overall is caused by diffusion due to the saturated dissolved hydrogen. The other part is the result of the supersaturated hydrogen concentration in the cathodic half-cell. Its percentage increased with current density and decreased with the increase of cathodic pressure. Current density effect loses importance at very high cathodic pressures. For alkaline electrolysis, the rise in current density slightly increases diffusional crossover as a consequence of supersaturation but the most important source of hydrogen into the anodic half-cell is the mixing of the electrolyte cycles.

The influence of the separating unit thickness on the anodic hydrogen content is studied. If the membrane thickness decreases, the hydrogen content strongly increases, in PEM electrolysis. At alkaline the hydrogen content is nearly independent of the separator thickness. For electrolysers that used Zirfon® as a separator, its reduction offers high potential for improving ohmic losses but the convective crossover would gain importance [19].

Zeradjanin and coworkers focused their research on finding improvements to reduce the large amount of electrical energy consumed by these electrochemical industrial processes, where gases were obtained. In that respect, they studied dimensionally stable anodes (DSA), which are commonly used for chlorine production and water electrolysis. Activities of four different samples of DSA were analysed and compared with respect to their geometrical properties in chlorine production. Little attention has been given to understand

morphological properties at the microscale and their impact on activity. Standard DSA coating consists of mixed oxides of titanium dioxide (TiO_2) and ruthenium dioxide (RuO_2) and supported on Ti. In general, it is assumed that a catalyst layer with a dense packing of active sites and fast electrode kinetics should guarantee high overall performance, although the importance of having access to the active sites is often overlooked. Morphology of the catalyst layer should influence the availability of the active sites during gas evolution. The anodes were prepared using titanium metal chips coated with TiO_2/RuO_2 mixed oxide in a stream of air at temperatures that did not exceed 600°C. RuO_2 is the active component of the coating since TiO_2 is the support matrix that ensures long term mechanical and chemical stability. The variation that the samples present is about the breaking conditions of the catalyst layer caused by thermally induced tensile stress. To identify the samples, the mass percentage of ruthenium (Ru) is established: 23.6%, 26.7%, 27.4%, and 23.4%. All the samples manifested different activities that suggested that the state of the surface is not reproducible with regard to their active surface area and/or their chemical composition. Thus, geometric effects (morphology and active surface area) are responsible for the discrepancy in the activity of the samples (changes in the efficiency of the mass transport). Samples have different active surface areas and number of active sites. The ones with the largest number exhibit the lowest activities and suffer the highest loss of activity with time. These researchers estimated the turnover frequency: the charge that passes through all the active sites per time unit divided by the charge needed to cover all the active sites with a monolayer of adsorbed species. Results showed that voltammetric surface charge and turnover frequency are inversely proportional. As the active surface area becomes larger, it seems that the accessibility of active sites becomes more difficult (inefficient use of available surface area). The "mud-crack" structure consists of islands and cracks. The size of the latter can be considered as porosities whose sizes influence mass transfer into the inner parts of the catalyst layers. Their width decreased in the order: 23.6% > 26.7% > 27.4% > 23.4% of Ru, which was exactly the trend obtained for turnover frequency and current density. So, the increments of "crack" widths decrease the voltammetric surface charge but increase the turnover frequency more rapidly. As a consequence, the overall activity of DSA is predominantly affected by the turnover frequency and not by a decrease of active surface area. The widths of the cracks determine the availability of the surface area for the reaction. Larger width contributes more accurately to effective mass transport and allows higher product turnover. If bubble nucleation proceeds inside the cracks, its growth would be limited and detachment should happen with smaller radii and more frequently. Their detachment permits the electrolyte to flow into the crack, thus enabling the pores in the inner parts of the coating to participate in the reaction. Due to the limited growth of bubbles, the excess energy delivered to solid/liquid interface (due to applying overpotential) is dissipated, amplifying oscillations. That leads to a higher frequency of detachment. The cracked regions locally exhibit higher conductivity. The random rupture of the catalyst layer or nonuniform local enrichment of Ru caused different crystallinities. As Ru has lower affinity for oxygen compared to Ti, the latter diffuses towards the outer surface of the catalyst coating to form TiO_2 while Ru remains at higher concentration in the inner layers [23].

Those researchers continue working with the same DSA electrodes to gain knowledge about the correlation of the local current distribution with the overall activity. To improve the efficiency of electrocatalytic gas evolution processes, it is necessary to take into consideration all the phenomena which contribute to energy losses [24]. Energy losses can be caused by

(i) activation overpotential;

(ii) ohmic drop at the anode or in the electrolyte;

(iii) concentration overpotential;

(iv) adherence of gas bubbles on electrode surface.

The surface morphology of DSA electrodes presented two regions: uniform and nonuniform. Besides the mud-crack structures, incomplete mud-cracks are also visible. Fluctuations of local activity could be possibly explained by an inhomogeneous distribution of activity on the electrocatalyst surface or deviations from the standard mud-crack morphology. Energy-dispersive X-ray (EDX) analysis shows that the samples have uniform chemical composition at the beginning and that surface segregation of ruthenium and enrichment with oxygen is a consequence of corrosion. Mud-crack zones exhibit a higher roughness than the zones with the incompletely formed mud-crack structures, a characteristic difference which is expected to influence local activity. It is known that "cracked" electrodes have much higher active surface than compact ones [25]. The mud-crack morphology is characterised by edges, where the local current density is expected to be very high. Incomplete mud-crack is an undesirable phenomenon. Local properties of the catalyst layer, which include fluctuations in morphology, are periodically repeated over the entire surface area. Different local activity could be distinguished between samples. Their activity trend is (crack size) $2\,\mu m > 1.0\,\mu m > 1.6\,\mu m > 0.5\,\mu m$, which resembles the amperometric curve obtained in the research article mentioned before [23]. Four important aspects to make reference to are the following:

(1) Spatial distribution of active sites influences the overall electrocatalyst performance.

(2) Overall activity increases as local current distribution becomes more uniform.

(3) Activity loss along time becomes less pronounced when distribution of activity is more uniform.

(4) Reproducibility of the catalyst preparation method is limited and the control of the properties of the coating is associated.

The perfect control of synthesis parameters shows a significant potential for improvement of coating's performance. It is possible to increase activity using the same loading and chemical composition by optimization of the synthesis. So, it is feasible to considerably improve the efficiency of gas evolving electrodes by getting better control over the synthesis parameters to obtain a more regular surface morphology and

Table 1: Chemical composition for stainless steel 316L.

Ni	Mo	Cr	S	P	Si	Mn	C
12.0	2.5	17.0	0.03	0.045	0.03	2.0	0.03

the use of catalysts with more uniform distribution inhibited loss of activity [24].

Water thermodynamic decomposition voltage is 1.23 V although the reaction does not occur before 1.65-1.7 V. Generally, cells operate at voltages of 1.8-2.6 V as a consequence of overpotential [7].

Overpotential is the increase of potential value of an electrode, with respect to the normal reversible potential. The decomposition potential of an electrolyte varies with the nature of the electrodes between which a solution is electrolysed, with the conditions of its surface, with its previous work, and with its homogeneity. The difference between the electrode potential, which is necessary to produce the passage of current and the equilibrium value when no current passes, is called the electrode overvoltage. This implies that there are overpotentials for the different products of electrolysis and for the various electrodes in which they are released [26, 27]. The overpotential may be assigned to three principal causes:

(i) Variation of the concentration of the reactants in the vicinity of the electrodes surface due to the passage of a current.

(ii) Capacity of the charge carriers to cross the interface.

(iii) Incorporation or extraction of atoms in a lattice of the electrode metal. In the case of metal-ion potentials, this could be hindered.

The total overpotential could be resolved into three additive components: concentration, transition, and crystallization. The concentration overpotential can be subdivided into diffusion and reaction [28].

Having these challenges in mind, this work focused on the reduction of the electrical resistance of the electrolyte that directly affects energy consumption. The electrical resistance of an object is an examination of its opposition to the passage of electric current. Its value is proportional to the cross-section area, the length of the current path, and the material resistivity of the conducting material [6]. According to that relation, the reduction of the space between electrodes (SBE) could lower the electrical resistance but, in this process, the formation of bubbles could modify this affirmation.

In this work the performance of two stainless steel 316L electrodes with straight-parallel topology were studied, in a special electrochemical cell. This cell simulated the same components and working conditions as those presented in an alkaline water electrolyser with the advantage of a system that allows modifying the distance between electrodes. This system, as it was designed, did not permit to capture the gases obtained but fulfil the object of this analysis. The distances proposed between electrodes are not the same in the case of the positive electrode (anode) to the separator and from the separator to the negative electrode (cathode). The reason why this is studied is that the stoichiometry of the reaction states that two mole of hydrogen and one mole of oxygen can be obtained per every two mole of water:

$$2H_2O + \text{electrical energy} \longrightarrow O_2 + 2H_2 \quad (1)$$

This situation was studied analysing nine different distances between electrodes and the separator, always trying to maintain twice the distance from the separator to the cathodic electrode. To the best of our knowledge, this is the first time that this kind of experiment is carried out.

The use of 316L stainless steel as material for the electrodes is based on its nickel content and its low cost. Although it is not the most efficient material to be used in these systems, it also allows determining its behaviour by establishing different distances between the electrodes and the separator, distance between electrodes and straight-parallel topology.

2. Materials and Methods

2.1. Electrode Preparation. The material used for the electrodes is stainless steel 316L, purchased from FAMIQ S.R.L. Their dimensions are 110 mm width, 2 mm depth, and 110 mm height. Table 1 presents the chemical composition for the stainless steel use.

2.1.1. Electrode Machining: Straight-Parallel Topology. The straight-parallel topology was selected as the geometric figure to increase the active area of the electrodes and improve, to some extent, the departure of the bubbles formed during the process. This topology is made by a universal milling machine, using a circular shaped high speed steel saw of 8 mm diameter and 1 mm thick (SINPAR). The dimensions selected for channels were 1 mm width, 0.5 mm depth, and 90 mm height for this topology. The incorporation of those channels increased the active area by approximately 50%, if compared to the same electrodes but in their flat original state.

The walls of the channels are responsible for the additional active area provided to the system. Bearing in mind the dimensions of the channels, 0.9 square centimeters were incremented, per channel. Considering the dimension of the flat original electrode, the active area is 99 cm^2. Adding channels to this area every 0.1 centimeters allows incorporating 55 channels and these represent an increase of 49.5 cm^2 of surface area [8].

2.1.2. Cleaning Treatment. After cutting the material purchased (stainless steel 316L) and mechanising the topology over its surface, it is necessary to clean it for taking off or eliminating organic substances. Those substances can be a residue of the manufacturing process, the cutting step or the mechanising of the channels. Those organic substances can block different portions of the active area of the electrodes, making those sectors useless for the reaction. All the electrodes were submitted to a cleaning treatment.

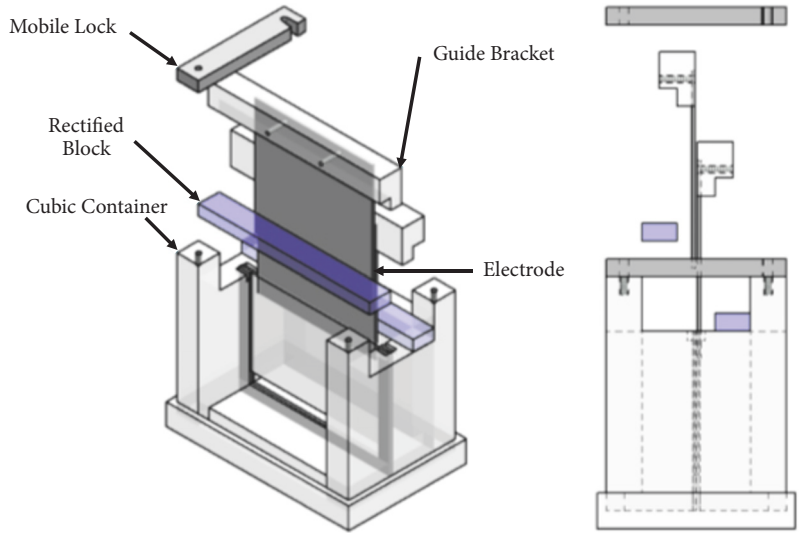

Figure 1: (a) Isometric exploded view and (b) side view of the electrolytic cell [29, 30].

That treatment consisted of five steps:

(i) Rinse off the electrodes with abundant tap water.

(ii) Wash the electrodes with a commercial abrasive cleaner.

(iii) Wash the electrodes with distilled water and allow them to dry.

(iv) Soak a filter paper with Acetone (Cicarelli Laboratory, Pro-Analysis A.C.S) and clean the complete surface of the electrode. Allow to dry, with the purpose of evaporating the solvent from the surface.

(v) Soak a filter paper with Ethanol (Soria 96) and use it to clean the electrode surface. Then allow to dry, with the purpose of evaporating the solvent.

After these cleaning steps, the electrodes were ready to be used in the corresponding mobile electrode electrolytic cell. It should be clarified that this procedure is carried out each time a given experiment is completed and the electrodes have to be removed from or put into the electrolytic cell.

The clean electrodes were incorporated to the electrolytic cell as will be explained below.

2.2. Mobile Electrode Electrolytic Cell. To establish the performance of the different space between electrodes, as well as the distance between the electrodes and the separator, an electrolytic cell totally constructed with crystal acrylic was used. The electrolytic cell is stagnant, which means that the same electrolytic solution is used along an experiment. The special characteristic of this cell was the possibility of establishing the position of the electrodes (the space between them) using a pair of rectified blocks. Figure 1 shows the isometric exploded view of the electrolytic cell [29, 30].

The components that constitute the electrochemical cell are container, rectified blocks, separator, guide brackets, screws, and mobile locks.

The rectangular container has the purpose to hold the electrolytic solution and it is where all the other components are placed. In its centre, there is a channel that ensures the vertical position of the material that is going to be used as separator and provides electrolyte tightness to the anodic and cathodic compartments. The different pairs of rectified blocks establish the space between electrodes. The pair of rectified blocks are made of acrylic and are positioned inside the container and along its largest walls and could be exchanged for the dimension necessary to obtain the desired distance between electrodes. The guide brackets have the function of holding the electrodes in a vertical position, perfectly parallel to each other and to the separator as well, in combination with two stainless steel screws. The screws act as electrical connectors. When all the pieces are in place, the system is secured by the use of the mobile locks. That is to say, the mobile locks maintained all the pieces fixed, along the experiment, keeping the spaces between electrodes under study. When the system is ready to be used, the distance between electrodes is checked with a gauge at three points: between the ends of the electrodes and at their centre. The description of the electrolytic cell was explained in more detail in Lavorante et al., 2014 [30].

2.3. Experiments in the Electrolytic Cell. An electrolytic solution of KOH 30% w/w (J.T. Baker, Pro-Analysis A.C.S., 87.0%), prepared with distilled water is used to carry out the experiments. Once the electrolytic solution was incorporated to the container of the electrolytic cell, one drop of a dispersion of sodium dodecyl sulfate was added to each compartment, to reduce the superficial tension of the solution. Zirfon® is the composite material used as separator.

This material is formed by ZrO_2 particles embedded in a polysulfone matrix. This material is synthesized by the film-casting technique. The thickness of the Zirfon® used, is 1 millimetre [13].

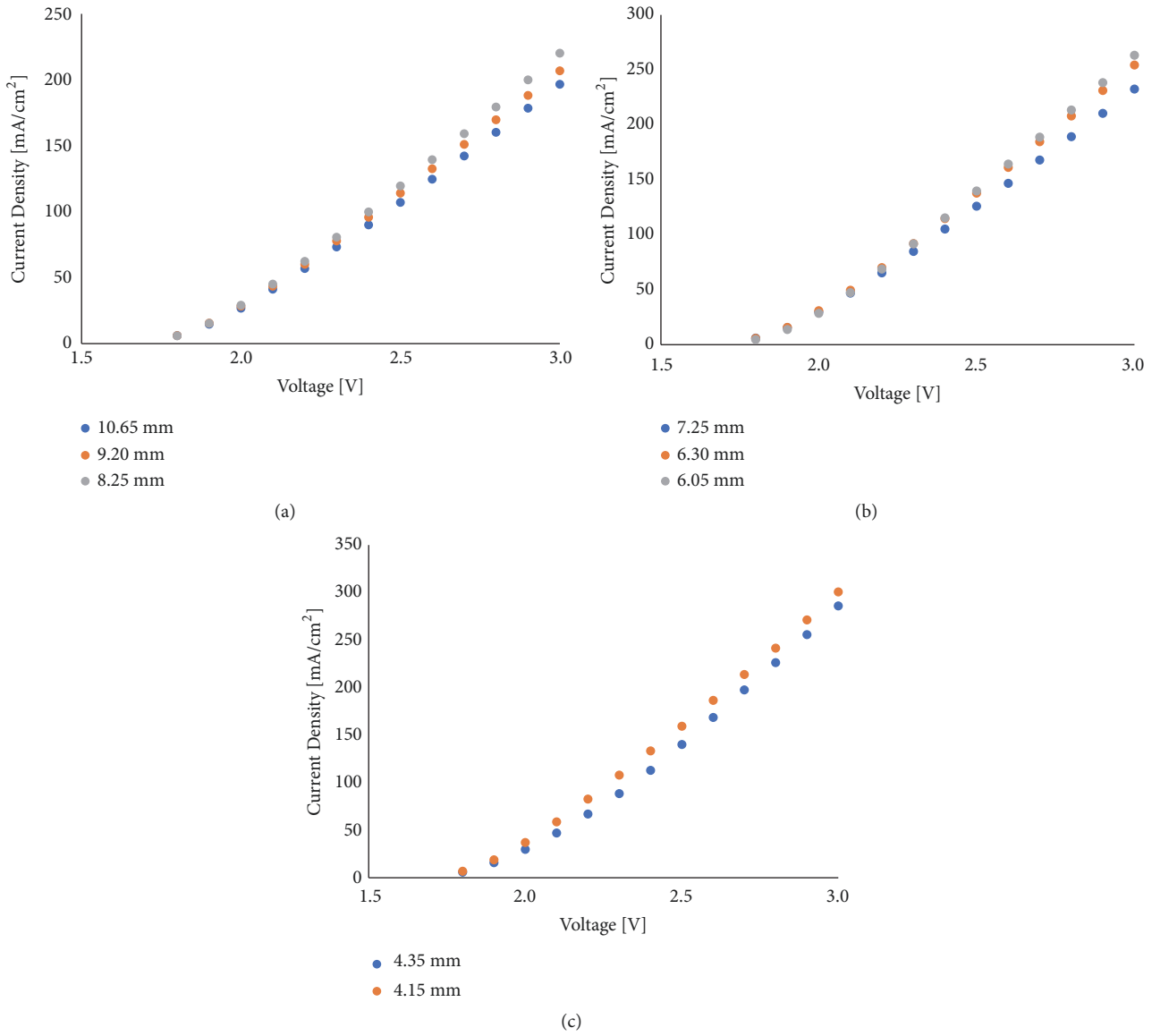

Figure 2: Polarization curves per unit area for the analysed distances between electrodes: (a) 10.65, 9.20, and 8.25, (b) 7.25, 6.30, and 6.05, and (c) 4.35 and 4.15 millimetres.

The electrical connectors were switched to a power source TDK-Lambda GEN20-76 System DC Power Supply (12.5 V/60 A,750 W). Current measurements were made at a certain potential between 0.0 and 3.0 V, changing the applied voltage differences 0.1 V every 30 s. Working conditions were atmospheric pressure and initial temperature of the electrolytic solution at 30.1°C. Voltage, current and temperature were the monitor parameters. The current for each potential was recorded at the end of each step (after every 30 s period) [8].

3. Results and Discussion

Nine different spaces between electrodes were studied: 10.65, 9.20, 8.25, 7.25, 6.30, 6.05, 4.35, 4.15, and 3.40 millimetres, and the behaviour of all the types of electrodes was analysed. Table 2 presents the space between the surface of the positive electrode and the surface of the separator (PES) and the space between the surface of the negative electrode and the surface of the separator (NES). As mentioned above, the cathode, in each of the determinations has approximately twice the distance from the separator of the anodic one, with the limitation presented by the use of rectified blocks. Each experiment (with a certain space between electrodes) was made three times and the results obtained were averaged together with the purpose of constructing the graphical representation. Standard deviation and standard error were calculated to obtain the error bars, to indicate how closely the average was likely to reflect the true values.

Figure 2(a) is the graphical representation of the polarization curves per unit area for the longest distances between electrodes: 10.65, 9.20, and 8.25 millimetres. Since the

Table 2: Total space between electrodes (SBE) analysed, spaces between the surface of the electrodes, and the surface of the separator.

SBE (mm)	PES (mm) Anode	NES (mm) Cathode
10.65	3.65	6
9.20	2.7	5.5
8.25	2.25	5
7.25	1.8	4.45
6.30	1.8	3.5
6.05	1.5	3.55
4.35	0.85	2.5
4.15	0.7	2.45
3.40	0.7	1.7

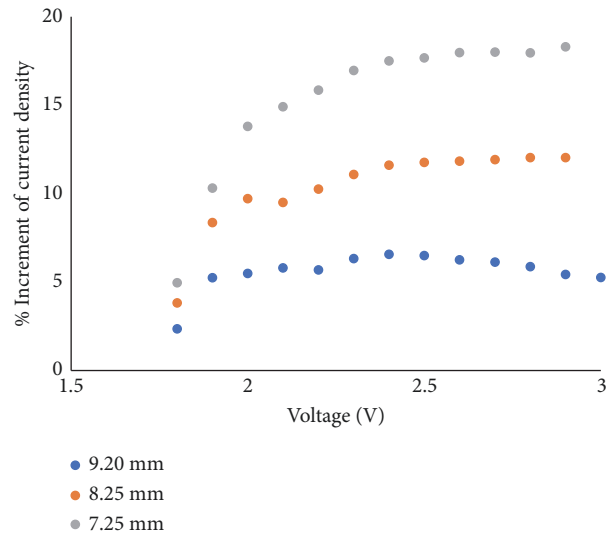

Figure 3: Percentage increment of current density analysed from the farthest distance between electrodes (10.65 mm).

standard error presented in the determinations is smaller than the marker used to identify the experimental values obtained (4.20 maximum value), it is not added to the graphical representation. As mentioned above the rectified blocks established the distance between electrodes but, in the cathode compartment, the distance between electrode and separator is almost twice the size of the anode.

Figure 2(b) is the graphical representation of the polarization curves per unit area for the distances between electrodes, 7.25, 6.30, and 6.05 millimetres, and Figure 2(c) for the closest ones: 4.35 and 4.15 millimetres. Once again, since the standard error presented in those determinations is smaller than the marker used to identify the experimental values obtained (3.20 and 4.4 are the maximum values, respectively), it is not added to the graphical representation.

As the distance between electrodes became smaller, the current density increased. As it was previously said, the electrical resistance of an object is an examination of its opposition to the passage of electric current. Its value is proportional to the cross-section area, the length of the current path and the material resistivity of the conducting material. As the length of the current path is smaller, so is the electrical resistance which allows increasing the current density in the system.

The smaller distance proposed in this analysis (3.40 mm) cannot be represented because the values of current obtained during the experiment did not remain stable due to the formation and departure of the bubbles.

From the current density results obtained for distances 9.20, 8.25, and 7.25 mm, it follows that, for each millimetre bringing the electrodes closer, the performance of the system improves by approximately 4%. If the percentage increment of current density is determined in each case from the value obtained subtracting the closest distance from the farthest one (fixed 10.65 mm), the results show that after a certain applied voltage difference, the system reaches a maximum increment value (see Figure 3).

This shows that the system manages to maintain an improvement in performance but much of the energy that is delivered is lost in the form of heat.

The gap between electrodes analysed in Figures 2(b) and 2(c) shows that the current density increased 3% approximately up to the last distance between electrodes proposed in the graphical representation (4.15 mm), where the increase was 15%.

To further analyse the difference between applying the same distance between electrodes or not, (the same distance at the cathodic and anodic compartment or the doubled distance for the cathodic one, respectively) another experiment was carried out. Arbitrarily, a distance between electrodes was selected, in this case 6.05 millimetres, and the experiment was developed under the same experimental conditions but the space between the surface of PES and the space between the surface of NES were the same (2.5025 mm). Figure 4(a) shows the results obtained after comparing both experiments.

If heat released was calculated as the current density by the applied voltage difference to both systems, it could be observed that for an equal amount of generated hydrogen the system with lower performance, the one with the same distance between electrodes and the separator, released more heat (Figure 4(b)).

From the analysis of the results presented in Figure 4(b), it can be said that at low current densities (<100 mA /cm^2), the presence of phenomena that contribute to the loss of energy (in the form of heat) cannot be appreciated due to the amount of product generated. When the current density increases (>100 mA/cm^2), the ohmic drop in the electrolyte and the concentration overpotential become more marked for the system, where the electrodes are at the same distance from the separator. The ohmic drop in the electrolyte is caused by the detachment of the gas bubbles formed. The concentration overpotential is due to the accumulation of dissolved gas in the vicinity of the electrode surface. As a consequence of these phenome, a greater voltage is required to obtain the same quantity of product and the energy losses result in a greater amount of heat released. Further research will be performed

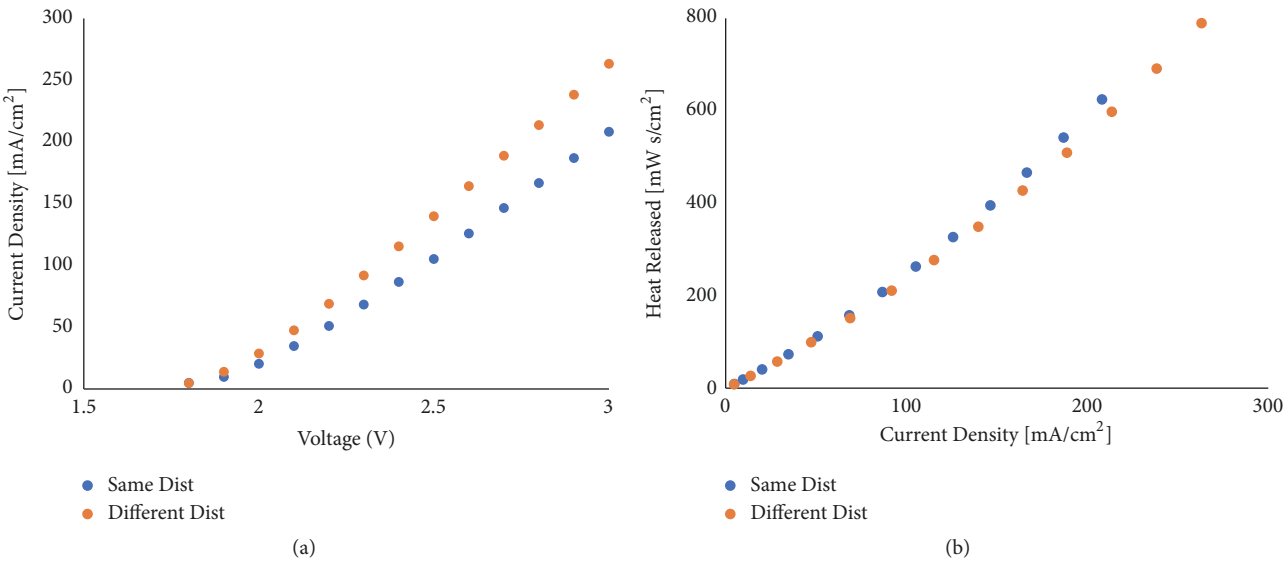

Figure 4: (a) Polarization curves per unit area for the same distance between electrodes and with different distances between the cathode and anode electrodes with respect to the separator and (b) heat released as a function of current density for the same systems.

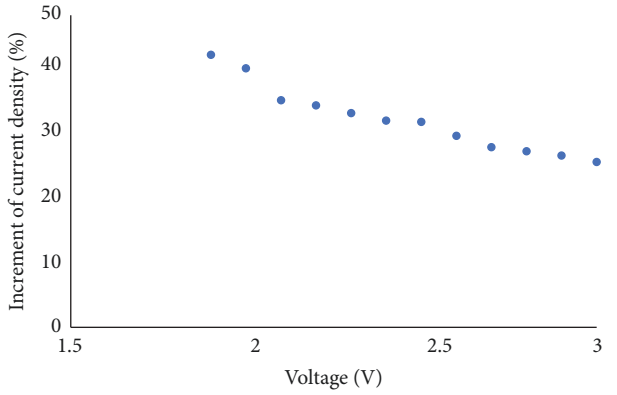

Figure 5: Increment of the current density as a function of the difference applied voltage.

to deepen the knowledge about these phenomena in this particular system.

The performance of the system presents better results when the distance between the electrode and the separator is not the same for each compartment. The current density increased by approximately 33% (average of all the determinations) for each different voltage applied. Figure 5 presents the graphical representation of that analysis.

4. Conclusions

From the nine different distances analysed between electrodes, where the negative electrodes are almost twice the distance from the separator than the positive ones, it can be said that the best performance was reached by one of the smallest distances proposed, 4.15 mm. In that distance the space between the surface of the positive electrode and the surface of the separator is 0.7 mm and the space between the surface of the negative electrode and the surface of the separator is 2.45 mm.

The smallest one 3.40 mm could not be analysed because during the experiment the values of current did not remain stable due to formation and departure of the bubbles.

When the same distance between electrodes was compared (systems with same and different distance between the electrodes and the separator), the one that had almost twice the distance (cathodic compartment) presented an increase in current density of approximately 33% with respect to that where both distances (from electrodes to separator) are the same. For an equal amount of hydrogen produced between those systems, the heat released was higher by the system with the same distance between electrodes and separator. At low current densities (< 100 mA /cm^2), the presence of phenomena that contribute to the loss of energy (in the form of heat) cannot really, be appreciated due to the amount of product generated. When the current density increases (> 100 mA/cm^2), the ohmic drop in the electrolyte and the concentration overpotential become more marked for the system, where the electrodes are at the same distance from the separator. As a consequence of these phenomena, a greater voltage is required to obtain the same quantity of product. Further research will be performed to deepen the knowledge about these phenomena in this particular system.

That indicates that the stichometry of the electrolysis reaction influenced the performance of the system. More research work has to be done in that respect but it is a starting point to continue with the study of the design improvements of this type of devices in order to reduce their energy consumption.

Data Availability

The data used to support the findings of this study are included within the supplementary information file (available here).

Disclosure

The manuscript is based on the poster that was presented at the 2nd International Symposium on Materials for Energy Storage and Conversion 2017, Ortahisar, Cappadocia, Turkey, the 26th and 28th September, 2017.

Conflicts of Interest

The authors declare that they have no conflicts of interest.

Acknowledgments

Authors want to thank the Defence Ministry and the Army Project Direction (DIEJ) for the given support. Authors are grateful to the Prototype Department of CITEDEF for the construction of the electrodes used in the experiments. The authors received funding from Argentinean Defense Ministry: 03 NAC 024/17 and 03EUV 032/15. This work is to honour the memory of our beloved mentor PhD. Juan Isidro Franco (12-09-1945 -13-07-2017) who has always accompanied us in the direction that our research will take or the one that we decided to follow. His untiring questions made us improve as researchers and, with it, the results of our work. He taught us that directing is not telling others what to do or how but to accompany them throughout the whole process to get the best out of them. We will miss our conversations on science and life very much. The Engineer Carla Yanina Reynoso made the determination of the trials together with Sc. Ba. María Jose Lavorante, who also planned the experiences and analysed the results.

Supplementary Materials

In this section are presented the results obtained from all the experiments carried out. Once the device is connected to the DC Power Supply, a potential difference sweep is carried out from 0 to 3 V and the current is recorded from every distance between electrodes studied, every 30 seconds. Then, the current results are processed, to obtain the current density with the active area of the electrodes. Finally, for each group of determinations, under the same working conditions, the average, the standard deviation, and standard error are calculated. *(Supplementary Materials)*

References

[1] R. F. de Souza, J. C. Padilha, R. S. Gonçalves, M. O. de Souza, and J. Rault-Berthelot, "Electrochemical hydrogen production from water electrolysis using ionic liquid as electrolytes: towards the best device," *Journal of Power Sources*, vol. 164, no. 2, pp. 792–798, 2007.

[2] S. M. Haile, D. A. Boysen, C. R. I. Chisholm, and R. B. Merie, "Solid acids as fuel cells electrolytes," *Nature*, vol. 410, no. 6831, pp. 910–913, 2001.

[3] S. J. Peighambardoust, S. Rowshanzamir, and M. Amjadi, "Review of the proton exchange membranes for fuel cell applications," *International Journal of Hydrogen Energy*, vol. 35, no. 17, pp. 9349–9384, 2010.

[4] R. F. De Souza, J. C. Padilha, R. S. Gonçalves, and J. Rault-Berthelot, "Dialkylimidazolium ionic liquids as electrolytes for hydrogen production from water electrolysis," *Electrochemistry Communications*, vol. 8, no. 2, pp. 211–216, 2006.

[5] J. O'M Bockris, B. E. Conway, E. Yearger, and R. E. White, *Comprehensive Treatise Electrochemistry*, vol. 3, Plenum Press, New York, NY, USA, 1981.

[6] K. Mazloomi, N. B. Salaiman, and H. Moayedi, "Electrical efficiency of electrolytic hydrogen production," vol. 7, pp. 3314–3326, 2012.

[7] V. M. Nikolic, G. S. Tasic, A. D. Maksic, D. P. Saponjic, S. M. Miulovic, and M. P. Marceta Kaninski, "Raising efficiency of hydrogen generation from alkaline water electrolysis—energy saving," *International Journal of Hydrogen Energy*, vol. 35, no. 22, pp. 12369–12373, 2010.

[8] M. J. Lavorante and J. I. Franco, "Performance of stainless steel 316L electrodes with modified surface to be use in alkaline water electrolyzers," *International Journal of Hydrogen Energy*, vol. 41, no. 23, pp. 9731–9737, 2016.

[9] K. Zeng and D. Zhang, "Recent progress in alkaline water electrolysis for hydrogen production and applications," *Progress in Energy and Combustion Science*, vol. 36, no. 3, pp. 307–326, 2010.

[10] S. M. Saba, M. Müller, M. Robinius, and D. Stolten, "The investment costs of electrolysis – A comparison of cost studies from the past 30 years," *International Journal of Hydrogen Energy*, vol. 43, no. 3, pp. 1209–1223, 2018.

[11] S. Srinivasan and F. Salzano, "Prospects for hydrogen production by water electrolysis to be competitive with conventional methods," *International Journal of Hydrogen Energy*, vol. 2, no. 1, pp. 53–59, 1977.

[12] P. Lettenmeier, R. Wang, R. Abouatallah, F. Burggraf, A. S. Gago, and K. A. Friedrich, "Coated stainless steel bipolar plates for proton exchange membrane electrolyzers," *Journal of The Electrochemical Society*, vol. 163, no. 11, pp. F3119–F3124, 2016.

[13] P. Vermeiren, W. Adriansens, J. P. Moreels, and R. Leysen, "Evaluation of the zirfon® separator for use in alkaline water electrolysis and Ni-H2 batteries," *International Journal of Hydrogen Energy*, vol. 23, no. 5, pp. 321–324, 1998.

[14] J. Xu, G. Liu, J. Li, and X. Wang, "The electrocatalytic properties of an IrO2/SnO2 catalyst using SnO2 as a support and an assisting reagent for the oxygen evolution reaction," *Electrochimica Acta*, vol. 59, pp. 105–112, 2012.

[15] M. Schalenbach, G. Tjarks, M. Carmo, W. Lueke, M. Mueller, and D. Stolten, "Acidic or alkaline? Towards a new perspective on the efficiency of water electrolysis," *Journal of The Electrochemical Society*, vol. 163, no. 11, pp. F3197–F3208, 2016.

[16] M. R. Kraglund, D. Aili, K. Jankova, E. Christensen, Q. Li, and J. O. Jensen, "Zero-gap alkaline water electrolysis Using ion-solvating polymer electrolyte Membranes at reduced KOH concentrations," *Journal of The Electrochemical Society*, vol. 163, no. 11, pp. F3125–F3131, 2016.

[17] A. Delvaux, Q. Van Overmeere, R. Poulain, and J. Proost, "Enhanced oxygen evolution during water electrolysis at de-alloyed nickel thin film electrodes," *Journal of The Electrochemical Society*, vol. 164, no. 12, pp. F1196–F1203, 2017.

[18] X. Lu and C. Zhao, "Electrodeposition of hierarchically structured three-dimensional nickel-iron electrodes for efficient oxygen evolution at high current densities," *Nature Communications*, vol. 6, pp. 1–7, 2015.

[19] P. Trinke, P. Haug, J. Brauns, B. Bensmann, R. Hanke-Rauschenbach, and T. Turek, "Hydrogen crossover in PEM and

Alkaline Water Electrolysis: mechanisms, direct comparison and mitigation strategies," *Journal of The Electrochemical Society*, vol. 165, no. 7, pp. F502–F513, 2018.

[20] H. Vogt, "Studies on gas-evolving electrodes: The concentration of dissolved gas in electrolyte bulk," *Electrochimica Acta*, vol. 30, no. 2, pp. 265–270, 1985.

[21] J. Chin Kwie Joe, L. Janssen, S. van Strelen, J. Verbunt, and W. Sluyter, "Bubble parameters and efficiency of gas bubble evolution for a chlorine-, a hydrogen- and an oxygen-evolving wire electrode," *Electrochimica Acta*, vol. 33, no. 6, pp. 769–779, 1988.

[22] J. St-Pierre, N. Massé, and M. Bergeron, "Dissolved oxygen concentration in a divided rotating cylinder electrode reactor," *Electrochimica Acta*, vol. 40, no. 8, pp. 1013–1024, 1995.

[23] A. R. Zeradjanin, F. La Mantia, J. Masa, and W. Schuhmann, "Utilization of the catalyst layer of dimensionally stable anodes—Interplay of morphology and active surface area," *Electrochimica Acta*, vol. 82, pp. 408–414, 2012.

[24] A. R. Zeradjanin, E. Ventosa, J. Masa, and W. Schuhmann, "Utilization of the catalyst layer of dimensionally stable anodes. Part 2: Impact of spatial current distribution on electrocatalytic performance," *Journal of Electroanalytical Chemistry*, vol. 828, pp. 63–70, 2018.

[25] R. Chen, V. Trieu, A. R. Zeradjanin et al., "Microstructural impact of anodic coatings on the electrochemical chlorine evolution reaction," *Physical Chemistry Chemical Physics*, vol. 14, no. 20, p. 7392, 2012.

[26] C. L. Mantell, *Engenieria Electroquimica*, McGraw-Hill Book Company, Editorial Reverte, Espana, 4th edition, 1980.

[27] J. O'M. Bockris and A. K. N. Reddy, *Modern Electrochemistry: An Introduction to an Interdisciplinary Area*, vol. 2, Editorial Reverte, Espana, 1980.

[28] G. Kortum, *Treatise on Electrochemistry*, Elsevier Publishing Company, London, UK, 2nd edition, 1965.

[29] M. J. Lavorante, C. Y. Reynoso, and J. I. Franco, "Water electrolysis with Zirfon® as separator and NaOH as electrolyte," *Desalination and Water Treatment*, vol. 56, no. 13, pp. 3647–3653, 2015.

[30] M. J. Lavorante, J. I. Franco, P. Bonelli, G. M. Imbrioscia, and H. J. Fasoli, *Springer Proceedings in Physics 155, Chapter 30*, 2014.